energies

MDPI

Article

Design and Analysis of Novel CO_2 Conditioning Process in Ship-Based CCS

Wentao Gong [1], Eryk Remiezowicz [2], Philip Loldrup Fosbøl [1] and Nicolas von Solms [1,*]

[1] Department of Chemical and Biochemical Engineering, Center for Energy Resources Engineering, Technical University of Denmark, Søltofts Plads, Building 229, DK-2800 Lyngby, Denmark
[2] Air Products, Kiełczowska 62A, 51-315 Wrocław, Poland
* Correspondence: nvs@kt.dtu.dk; Tel.: +45-45252867

Abstract: In this work, CO_2 conditioning processes for ship-based CCS sequestration are modelled using the software APSEN HYSYS V11. This study uses the captured CO_2 gas from the 3D project as the feed. The feed stream contains water, H_2S, and CO as contaminants. The purification processes for dehydration, desulfurization, and CO removal are reviewed. Two liquefaction approaches, the open-cycle and the closed-cycle liquefaction, are modelled and compared for transport pressures 7 and 15 bar. It is found that the energy requirement of the open-cycle process is higher than that of the closed-cycle liquefaction process. For the closed-cycle design, two refrigerants, ammonia and propane, are considered. Results show that the energy requirement of the process using ammonia is lower than that of propane. When comparing the two transport pressures, it is found that liquefaction at 15 bar requires less energy than 7 bar. On top of that, both refrigerants are unsuited for the liquefaction of CO_2 at 7 bar, as their operating pressures are below 1 atm. Several optimization concepts are tested on the closed-cycle liquefaction design. The net power consumption of the closed-cycle liquefaction is reduced when CO_2 is precooled using the intermediate pressure ammonia streams and the cold from the CO stripper.

Keywords: CO_2 capture; DMXTM process; CO_2 conditioning; CO_2 liquefaction; CCS hub Dunkirk

Citation: Gong, W.; Remiezowicz, E.; Fosbøl, P.L.; von Solms, N. Design and Analysis of Novel CO_2 Conditioning Process in Ship-Based CCS. *Energies* **2022**, *15*, 5928. https://doi.org/10.3390/en15165928

Academic Editor: Nikolaos Koukouzas

Received: 18 July 2022
Accepted: 10 August 2022
Published: 16 August 2022

1. Introduction

During the last decade, carbon capture, utilization, and storage (CCUS) technologies received increasing attention from our society as solutions to reduce CO_2 emissions and mitigate global warming. Currently, CCUS technologies are being progressively researched, demonstrated, and implemented in power plants and other industries around the globe. This study is part of the EU H2020 project "DMX^{TM} Demonstration in Dunkirk (3D)". The 3D project aims to reduce the CO_2 emissions from the steelmaking industry, which currently make up around 5% of the global industrial CO_2 emissions [1]. The main objectives of the 3D project are to demonstrate the efficiency of the DMX^{TM} process, developed by IFP Energies Nouvelles (IFPEN), and to implement the first CCS units at ArcelorMittal's steel production site in Dunkirk.

The liquefaction of CO_2 is an essential process between the capturing process and safe tank transport. For tank transport, CO_2 needs to be kept at its liquid state at a low pressure. A. Aspelund et al. suggested that CO_2 is most efficiently transported at approximately 6.5 bar and −51.2 °C [2]. However, liquefaction at such pressure is very energy consuming and hence not optimal for the CCS sequestration. The optimal transport conditions shall be evaluated from both the cost of ship transport and the CO_2 conditioning process. For the 3D project, a detailed analysis of ship transport is conducted by [3].

The energy requirement for the liquefaction process is typically 90–120 kWh/ton CO_2 [4]. This corresponds to approximately 4% of total power produced at a power plant [5]. Despite the fact that CO_2 liquefaction is an energy-consuming process, most CCUS research

is devoted to the capture, transport, and storage processes, and the conditioning processes are comparatively overlooked.

A few recent studies compared the energy consumption and cost of various liquefaction approaches.

H. Deng et al. (2019) modelled a closed-cycle CO_2 liquefaction process with ammonia as the refrigerant. In their design, the captured CO_2 gas is compressed to a high pressure at which it is liquefied using ammonia. Afterward, the liquefied CO2 is expanded to the transport pressure. They compared the cost of the process for CO_2 transport pressures from7 to 70 bar and found that the liquefaction cost is highest at 7 bar, while the minimum is obtained at around 40–50 bar [6]. However, transporting CO_2 at high pressures can be costly. The most desired transport pressures are around 7 to 20 bar. Therefore, optimal process configurations to produce liquid CO_2 in this pressure range are needed.

A. Alabdulkarem et al. (2012) compared different open- and closed-cycle CO_2 liquefaction designs for pipeline transport. However, the CO_2 liquefaction pressure investigated in their study is 6 bar, at which the saturation temperature is −57 °C [7]. Liquefaction at such low temperatures is impractical using most refrigerants, including ammonia. In addition, their study focuses on producing liquid CO_2 at high transport pressures, which is not suitable for ship transport.

L. Øi et al. (2016) also compared standard open and closed CO_2 liquefaction processes with ammonia as the main refrigerant. Although they found that the multistage refrigeration process has the lowest net duty and operating cost, their process parameters and configurations are not optimized [8].

Y. Seo et al. (2016) compared three open-cycle designs (Linde Hampson system) with the closed-cycle designs for ship-based transport. They calculated the CAPEX and OPEX of the designs, and found that the closed-cycle has the lowest life cycle cost (LCC) [9].

Although the conventional refrigeration technologies for CO_2 liquefaction have been compared, no study focuses on optimizing the open and closed CO_2 liquefaction processes at the most efficient transport pressure range from 7 to 15 bar [9–13]. S. Roussanaly et al. (2021) compared the transport cost of 7 and 15 barg shipping. They examined different scenarios, including transport between harbors versus transport to an offshore site, CO2 pressures prior to conditioning, impurities, and ship capacities. They concluded that while transporting CO_2 at 15 barg is the most technologically mature, in most cases, the 7 barg option is more cost-efficient [12]. Therefore, more research on optimizing CO2 liquefaction processes in this pressure range is needed. In this study, the total power consumption of various CO_2 liquefaction process concepts, which is the main process parameter for calculating the OPEX of gas liquefaction processes, is compared and optimized.

Captured Gas Compositions

The feed stream used in this work is a CO_2 gas captured from a steel mill in Dunkirk. The process flowsheet for the steel mill is not shown here. The DMX^{TM} CO_2 capture process that is used to capture the CO_2 gas is described in detail in [14,15]. The steam compositions are shown in Table 1. The steam pressure is 6 bar, and the temperature is 60 °C.

Table 1. Captured gas compositions.

Mass Flow Rate	Value
CO_2 mass flow rate (tons/h)	123.1253
H_2O mass flow rate (tons/h)	1.8469
H_2S mass flow rate (tons/h)	0.0043
CO mass flow rate (tons/h)	0.0235
Total (tons/h)	125

2. Gas Purification

2.1. Introduction

In the conditioning process, impurities such as H_2O, H_2S, and CO are removed. Water can cause corrosion to the equipment and increase both CAPEX and OPEX of the process. Additionally, water can form hydrates, which can scale and cause a blockage within the system. The corrosion happens when water comes into contact with the surface of the equipment. L. W. Diamond and N. N. Akinfiew (2003) found that the water solubility in gaseous CO_2 decreases with higher pressure and lower temperature [16]. Furthermore, CO_2 and H_2S can be dissolved in water, forming carbonic and hydrosulfuric acid and accelerating corrosion [17,18]. Removing water in the early stage of the conditioning process can be advantageous. The formation of CO_2 and H_2S hydrates is well-studied in the literature [19,20]. Hydrate species can form in gas and liquid over a wide range of temperatures and pressures. Both H_2S and CO are toxic and should be removed. The 3D project collaborates with the Northern Light project, which manages the CO_2 storage site located in Norway. The purity requirement for H_2O, H_2S, and CO in the CO_2 gas requested by the Northern Light project are listed in Table 2.

Table 2. Purity requirements for CO_2 storage.

Contaminants	Concentration (ppm)
H_2O	≤ 30
H_2S	≤ 9
CO	≤ 100

2.2. Gas Dehydration

Several technologies for gas dehydration are available in the literature. The most commonly used ones for CCS operations are adsorption and absorption columns and VLE separation drums. Kemper et al. (2014) evaluated those concepts and constructed a guideline for choosing the appropriate CO_2 dehydration process. According to their study, adsorption using molecular sieves can easily reduce the moisture of CO_2 gas to under 1 ppm, whereas absorption using TEG can reduce moisture to about 30 ppm. However, molecular sieves can be sensitive to corrosion, especially when impurities such as H_2S are present. In such a case, more corrosion-resistant material is required. The CAPEX and OPEX of these columns can vary a lot because they can be highly customizable. High pressure is generally preferred, as it decreases the gas volume flow, reducing the columns' size. The costs also increase with moisture content. They suggest combining different dehydration strategies, such as offloading the water content using separation drums before sending the gas to the finer dehydration unit [21].

2.3. Gas Desulfurization

There are several technologies for the removal of H_2S from the captured CO_2 gas. The absorption method uses physical and chemical solvents to dissolve or react with H_2S. For instance, the Rectisol process is an absorption process where chilled methanol is used as the physical solvent. In this case, the separation is carried out based on the solubility between H_2S and CO_2 [22]. Chemical absorbents are usually amine and carbonate solutions that react with H_2S and CO_2 to form weak compounds. Both physical and chemical solvents are regenerative.

Solid adsorbents such as metallic oxides react only with H_2S. A well-known adsorption process is the iron sponge process, with ferric oxides as the adsorbent. In this case, hydrogen sulfide reacts with ferric oxide to form ferric sulfide. The ferric oxide can be regenerated using air.

Using activated carbon is an expensive but effective method to remove H_2S. There is impregnated carbon and non-impregnated carbon. The impregnated, activated carbon is usually treated with different chemicals that give the carbon surface additional functionali-

ties. The impregnated activated carbon has a loading capacity of up to 0.15 g/g activated carbon, whereas non-impregnated activated carbon only has a loading capacity of up to 0.02 g/g activated carbon [23].

Most recently, newer technology for H_2S removal was developed. S. Villadsen (2019) studied the H_2S removal method using an electro scrubber [24]. In this method, a highly oxidative gas, such as Br_2 or Cl_2, reacts with H_2S to produce sulfur. The dissolved halogens are then regenerated in an electrolytic cell. The advantage of using this technology is that it is cheap and effective.

2.4. CO Removal

CO is a volatile gas and can be removed thermodynamically. In this work, a reboiled stripper is modelled in ASPEN HYSYS V11 to reduce the content of CO in the liquid CO_2 from 300 ppm to 100 ppm. In the simulation, the reboiler ratio of the stripper is adjusted to remove excess CO. The separation yields an overhead product of 99.1% CO_2. It is, therefore, necessary to adjust the stage number to reduce the flowrate of the overhead product. See Figure 1.

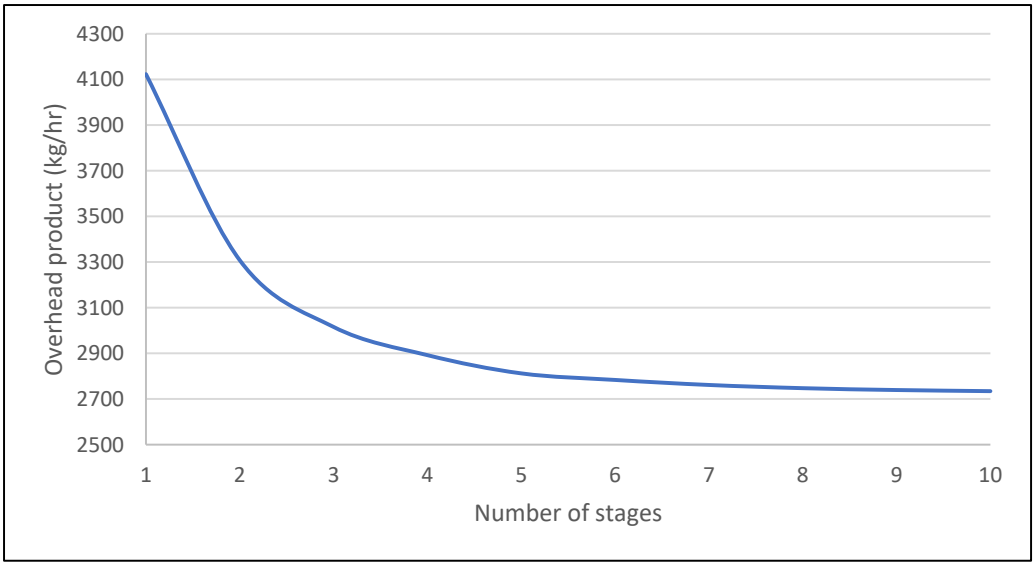

Figure 1. Effect of the stripper stage number on the flow rate of the overhead product.

Figure 1 shows that above five stages, the change of the overhead product flow rate is almost neglectable. Therefore, we assume in this study that the number of stages of the reboiled stripper is five. The calculated reboiler duty for the reboiled stripper is 887 MJ/h.

3. CO_2 Liquefaction

3.1. Introduction

In this section, process designs based on the open- and closed-cycle liquefaction concepts are modelled for the two transport pressures: 7 bar and 15 bar. The simulation software used in this work is ASPEN HYSYS V11. The thermodynamic model is the Peng–Robinson equation of state. In addition, the following assumptions are made:

- The compressor adiabatic efficiency is 80%, which has been used by other authors [7];
- Turbine isentropic efficiency is set to be equal to the compressor adiabatic efficiency, which is 80%;
- The temperature of the hot streams after coolers is set to 30 °C;
- The pressure drop in the ammonia side of the heat exchangers is 1 kPa. In the coolers and CO_2 side of the heat exchangers, the pressure drop is 10 kPa;
- The maximum compressor ratio is 4;
- The pinch temperature in heat exchangers is 5 °C.

For simplicity, it is also assumed that the dehydration and desulfurization processes, represented by the two component splitters, remove all water and hydrogen sulfide from the system. The dehydration process is placed at the beginning of the conditioning process, as water may cause damage to the equipment. The desulfurization process is placed after the first compressor stage, at which the pressure of the CO_2 gas is increased to 7 or 15 bar. The volume flow rates of the CO_2 stream under these two pressures are reduced by 19% and 63%, respectively, compared to 6 bar.

3.2. Open-Cycle Liquefaction

In the open-cycle design, the captured CO_2 gas is compressed and cooled. The liquefaction is then achieved by expanding the gas to the two-phase region. The expansion can be completed with either a control valve or a turbine. Both alternatives are explored.

3.2.1. Open-Cycle Liquefaction with a Control Valve

In this design, the captured gas is firstly cooled to 30 °C. Then, the gas is dehydrated using a VLE separator and a component splitter, which represents a dehydration method discussed in Section 2. After that, the pressure of the gas stream is increased to the transport pressure, i.e., 7 or 15 bar, using one compression stage. This is necessary to prevent any backflow when mixing the gas stream with the recycle stream, which is produced during the expansion of the pressurized CO_2. Next, H_2S is removed from the system. After mixing the captured CO_2 gas with the recycle stream, the combined stream is compressed to a high pressure using three compression stages. After the third compressor, the gas is cooled to 30 °C using cooling water. The gas is further cooled in a heat exchanger, which transfers the heat from the high-pressure CO_2 stream to the recycling stream. The heat exchanger is designed based on the outlet temperature of the recycling stream, which is fixed to 25 °C. Finally, the gas is expanded to the transport pressure. During the expansion, the vapor product is returned for recompression, while the liquid is sent to the CO stripper. The process flow diagram of this process is shown in Figure 2. The P–H diagram of CO_2 in the open-cycle liquefaction process is constructed using the software CoolPack. See Figure 3.

Adjustable parameters for this process are the high-end pressure (the pressure before expansion) and the pressure ratios. The pressure ratios can be varied to identify the minimal required total compression power using the optimizer feature in ASPEN HYSYS.

The objective function used for the optimization is:

$$\text{minf}(PR_i) = \sum W_{Comp} \text{ for } i = 1, \ldots, n \quad (1)$$

where PR_i is the pressure ratio in each compressor and W_{Comp} is the compressor power of each compressor. The net power is then minimized.

The high-end pressure affects the process in two ways. (1) Increasing the high-end pressure increases the pressure ratio of the compressors. (2) Increasing the high-end pressure improves the liquid split, hence, reducing the flow rate of the recycle stream. See Figure 4.

The total compressor power goes up with increasing compressor ratio, but goes down with decreasing flow rate. The optimal high-end pressure is, therefore, a result of a trade-off. The simulation of the open-cycle liquefaction process is made for the high-end pressure, from 75 bar to 95 bar. It is found that for the 15 bar transport case, the optimal high-end pressure is 85 bar. Above this pressure, the total compression power of the process begins to increase.

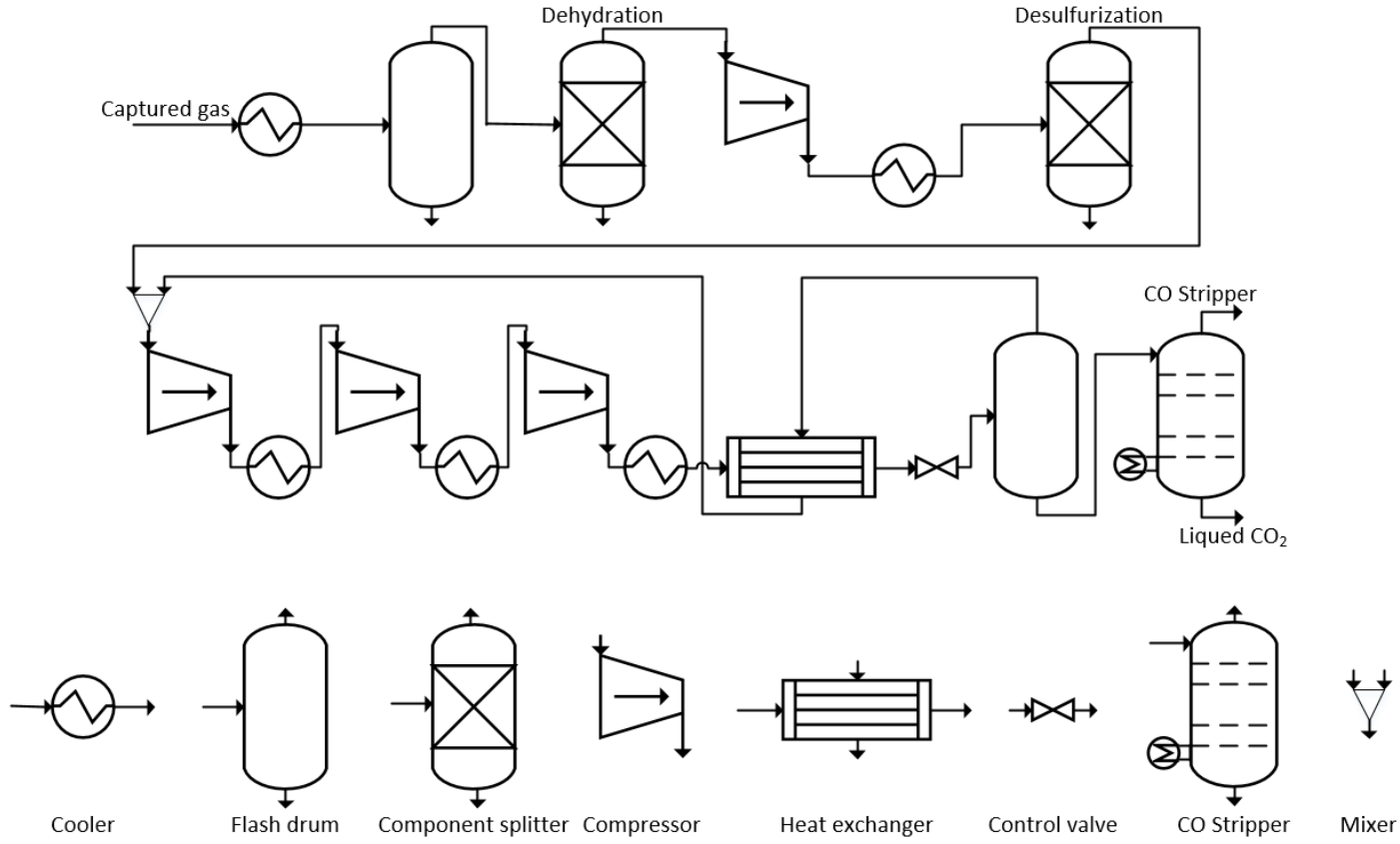

Figure 2. Process flow diagram for the open-cycle liquefaction design with a control valve.

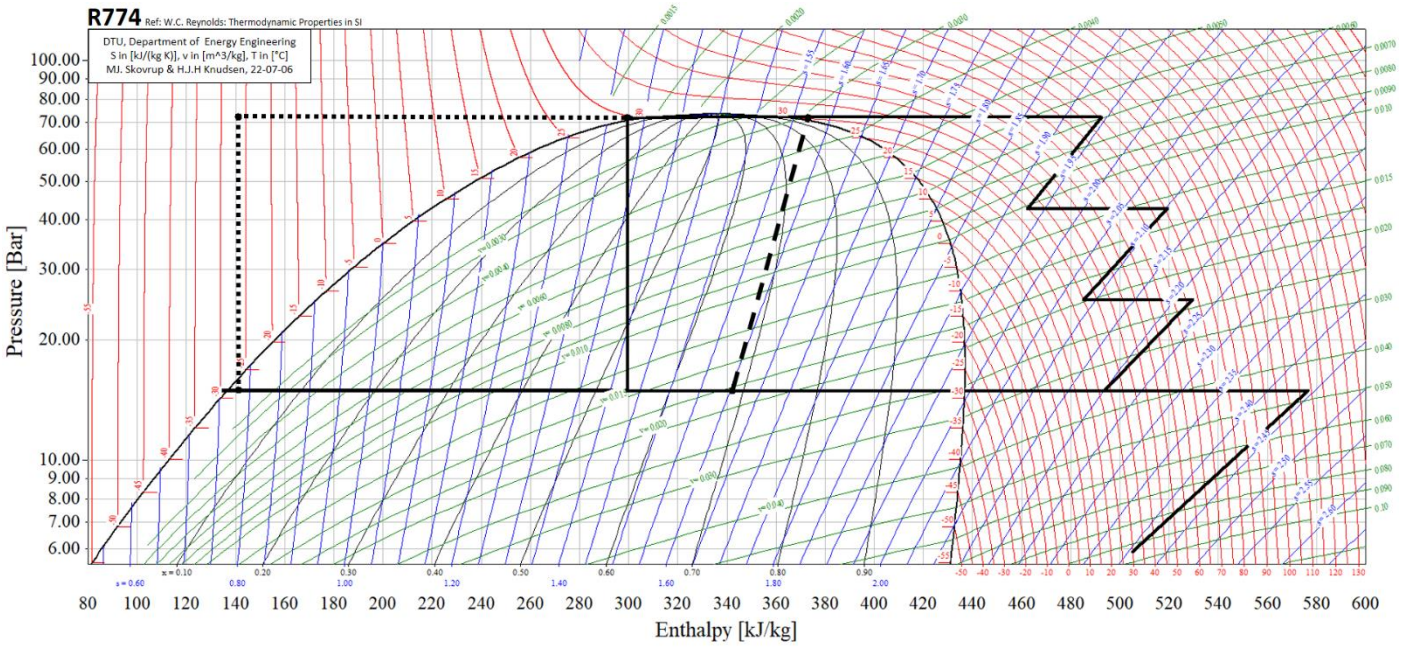

Figure 3. P–H diagram of CO_2 in the open-cycle liquefaction process. The high-end pressure in this case is 72 bar. The black curve shows the open-cycle liquefaction with the control valve. The dashed line shows the expansion with a turbine. The dotted lines show the expansion at −23 °C. Redlines: Isotherms, blue lines: Isentrops, green lines: Isochors.

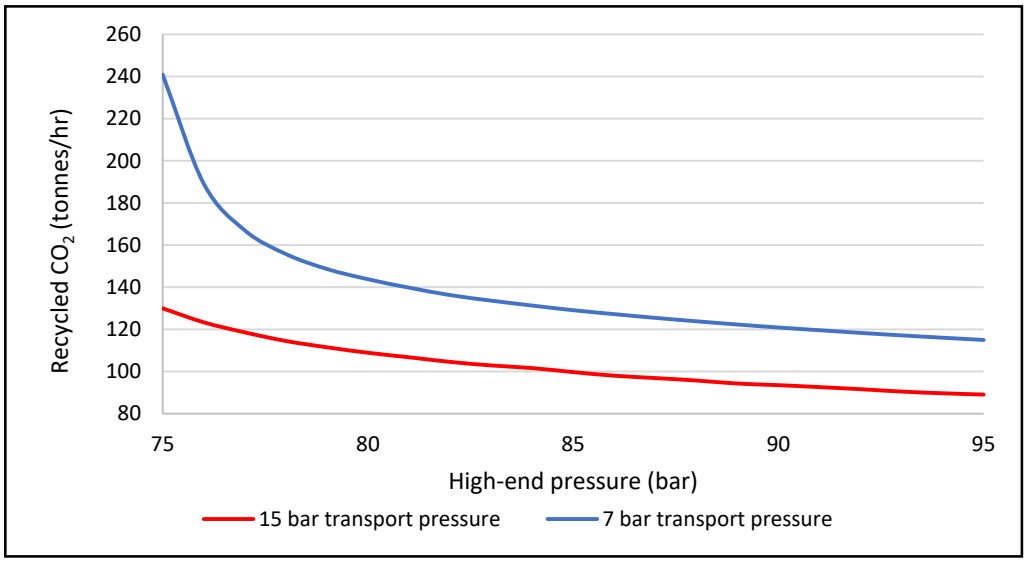

Figure 4. Effect of the high-end pressure (x-axis) on the CO_2 recycling flow rate (y-axis).

Figure 5 shows the effect of the high-end pressure on the total compressor power of the open-cycle liquefaction design. It is shown that at low transport pressures, the total compressor power is significantly improved by increasing the high-end pressure. However, this is not the case for higher transport pressures. The results for 85 bar as the high-end pressure are summarized in Table 3. It is found that the power consumption of the open-cycle liquefaction design is approximately 29% less for the 15 bar transport case than that of the 7 bar transport case. This is mainly due to the fact that in the 7 bar transport case, the recycled stream is expanded to a lower pressure than the 15 bar transport case.

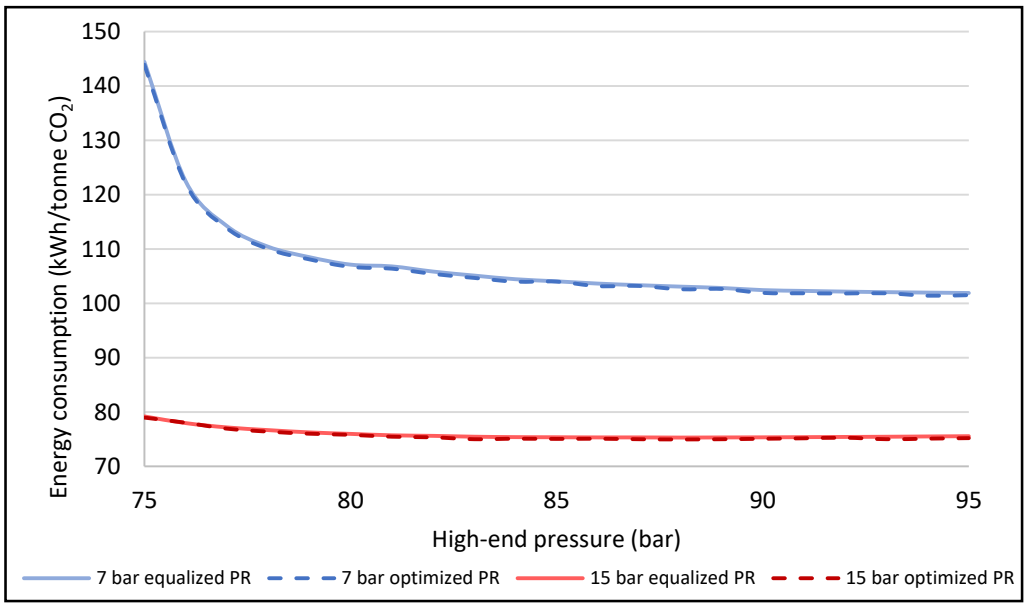

Figure 5. High-end pressure (x-axis) against total compressor power (y-axis) for open-cycle liquefaction. The full lines shows the simulation results with equal pressure ratios and the dashed lines are for optimized pressure ratios.

Table 3. Results of the open-cycle liquefaction design with the high-end pressure of 80 bar.

Design Cases	Compressor Power (MW)	Electric Energy per Ton CO_2 (kWh/ton)	Cooling Duty (GJ/hr)
7 bar	12.8	103.6	104.1
15 bar	9.3	75.9	86.5

3.2.2. Open Cycle Liquefaction with a Turbine

The control valve in Figure 1 can be replaced by a turbine. Since the inlet stream to a turbine must be a gas, the temperature and pressure must be fixed at 30 °C and 72 bar, respectively. For this design, the flow diagram in Figure 1 is modified by removing the heat exchanger and fix the high-end pressure to 72 bar. See Figure 6.

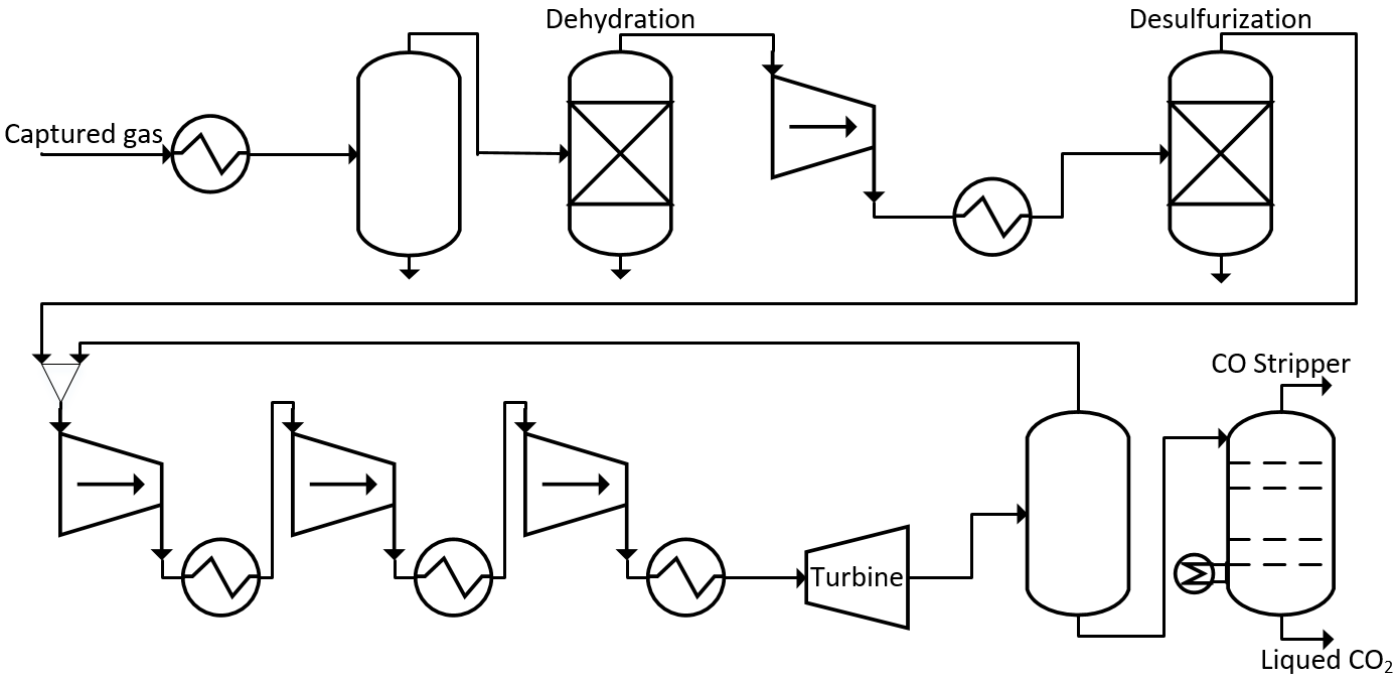

Figure 6. Process flow diagram for the open-cycle liquefaction design with a turbine.

The expansion of CO_2 is illustrated in Figure 2 with the dashed line. The starting point of the expansion process is on the vapor side of the two-phase region. For 15 bar transport case, a 32% liquid split is achieved due to work performed by the gas on the turbine. The results of this process are shown in Table 4.

Table 4. Results of the open-cycle liquefaction design with a turbine.

Design Cases	Compressor Power (MW)	Turbine Work (MW)	Net Power Required (MW)	Electric Energy per Ton CO_2 (kWh/ton)	Cooling Duty (GJ/h)
7 bar	18.4	5.7	12.7	103.1	103.7
15 bar	12.6	3.3	9.3	75.8	86.4

3.2.3. Open-Cycle Liquefaction with a Turbine and a Valve

In this design, the CO_2 liquid split is improved by reducing the temperature of the CO_2 stream before the expansion process. This is performed by splitting the high-pressure CO_2 stream into two different streams. For example, in the 15 bar transport case, the first stream is cooled to −23 °C, and then expanded through a valve. The liquid split through the valve

is 96%, due to the low starting temperature. The second stream is expanded through a turbine to the transport pressure. The liquid produced from the turbine is separated as the product, while the vapor split is used to cool the first CO_2 stream. The split ratio between the two streams is calculated to optimize the heat exchanger between the two streams. That is, the first CO_2 stream is cooled to −23 °C and the vapor CO_2 stream from the turbine is heated to 25 °C. For the 15 bar transport case, the CO_2 split ratio to the turbine is 86.6%. To further optimize the process, a cooler is placed after the splitter to liquefy the first CO_2 stream. See Figure 7. The results of this design are shown in Table 5.

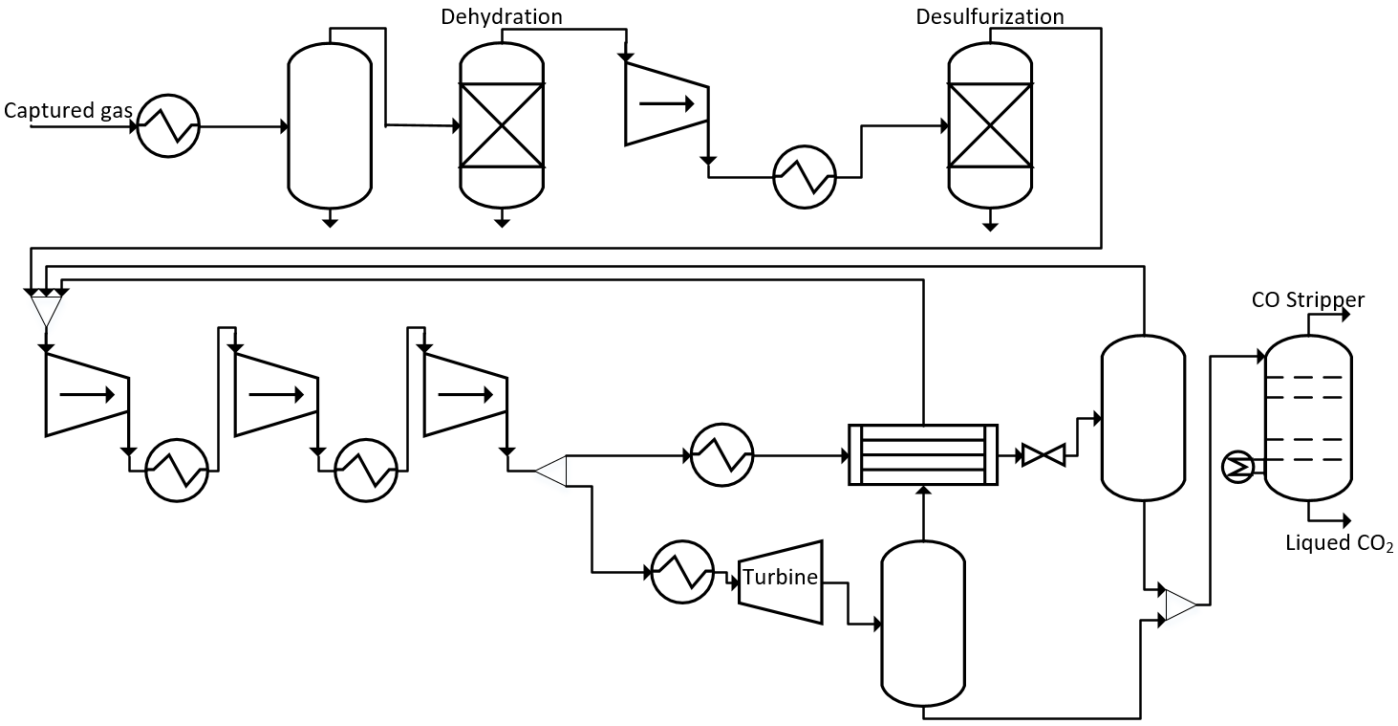

Figure 7. Process flow diagram for the open-cycle liquefaction design with a turbine and a valve.

Table 5. Results of the open-cycle liquefaction design with a turbine and a valve.

Design Cases	Compressor Power (MW)	Turbine Work (MW)	Net Power Required (MW)	Electric Energy per Ton CO_2 (kWh/ton)	Cooling Duty (GJ/h)
7 bar	13.6	3.0	10.6	85.7	96.3
15 bar	10.5	2.0	8.4	68.6	83.3

3.3. Closed-Cycle Liquefaction

3.3.1. Closed-Cycle Liquefaction Base Design

In the closed-cycle liquefaction design, an external refrigerant is used to liquefy CO_2. The boiling point of CO_2 at 7 bar is −49 °C, and at 15 bar is −28 °C. Assuming the pinch temperature is 5 °C, the refrigerant used in the 7 bar case is expanded to −54 °C and −33 °C in the 15 bar case. In this work, ammonia is chosen as the refrigerant. Propane is also modelled for comparison purposes.

Ammonia is a commonly used refrigerant with a global warming potential of zero. At −33 °C, the saturation pressure of ammonia is one atm. However, for −54 °C, the saturation pressure is only 0.3 bar.

An alternative choice is propane. Propane has a GWP of 3.3 [25]. At −33 °C, the saturation pressure of propane is 1.5 atm, and at −54 °C is 0.6 atm. Liquefaction at 7 bar is, therefore, not feasible with both refrigerants.

Unfortunately, most refrigerants have very low operating pressures for both design cases and are therefore not considered. In addition, refrigerants such as Freons are also not considered, as they have very high GWP. The process flow diagram of the closed-cycle liquefaction is shown in Figure 8.

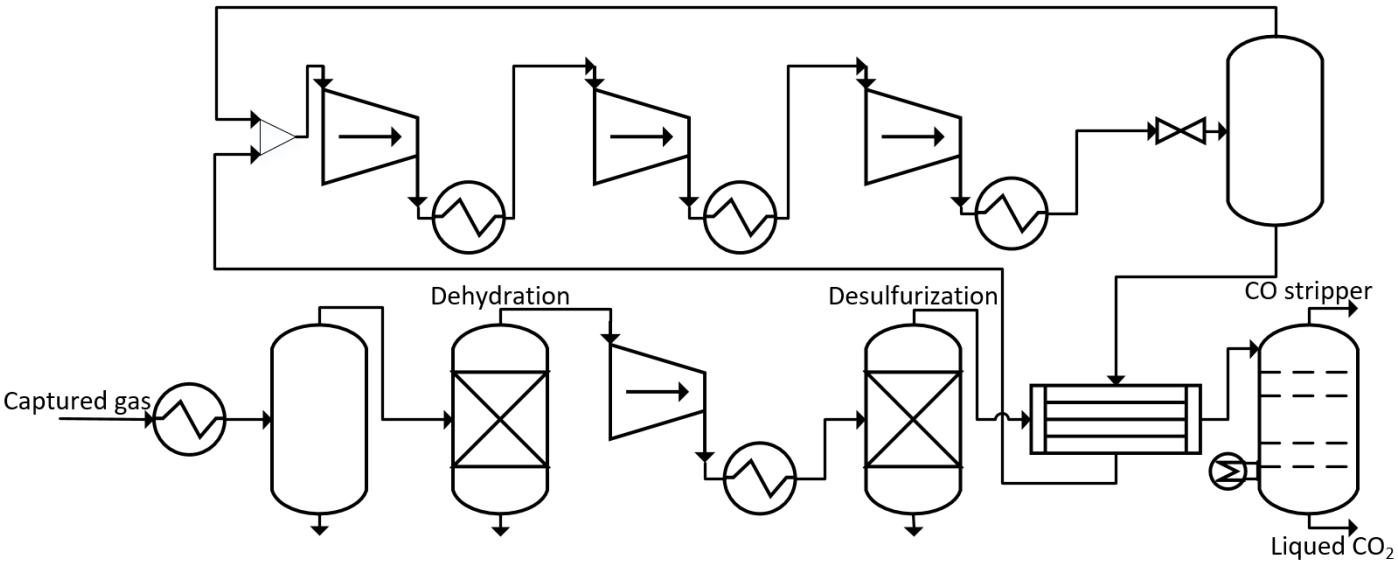

Figure 8. Process flow diagram for the closed-cycle liquefaction design.

In this design, the captured CO_2 gas is precooled to 30 °C and dehydrated. After that, it is compressed to the transport pressure. After H_2S is removed from the gas, the gas is liquefied in a heat exchanger. Finally, CO is removed from the gas in a stripper.

The refrigerant cycle consists of three compressor stages. The feed to the first compressor has a very low temperature. Therefore, the compressor ratio of the first compressor is set to 4. The remaining two compressors are designed with identical pressure ratios. The final pressure after the third compressor is 11.6 bar. At this pressure, the ammonia stream can be liquefied using cooling water. Cold ammonia at −33 °C can then be produced by expanding the liquid ammonia from 11.6 bar to 1 bar. The P–H diagrams of ammonia are shown in Figure 9.

Figure 9 shows that ammonia is compressed from 1 bar to 11.6 bar with three compression stages. It is then liquefied with water, and expanded again to 1 bar. The heat curve for the heat exchanger is shown in Figure 10.

Figure 10 shows that the vaporization heat of liquid ammonia is used to cool and liquefy CO_2. CO_2, on the other hand, is cooled from 30 °C to −28 °C, where it is liquefied. The results for the two refrigerants are shown in Table 6.

Comparing the designs of the two transport cases, 15 and 7 bar, with ammonia as the refrigerant, the 15 bar design case consumes around 23% less energy than the 7 bar design case. Additionally, the 7 bar designs cannot be achieved with the refrigerants, as the operating pressures of both refrigerants are below one bar. By comparing the designs with ammonia and propane, it is shown that the designs with ammonia require less energy compared to the designs with propane.

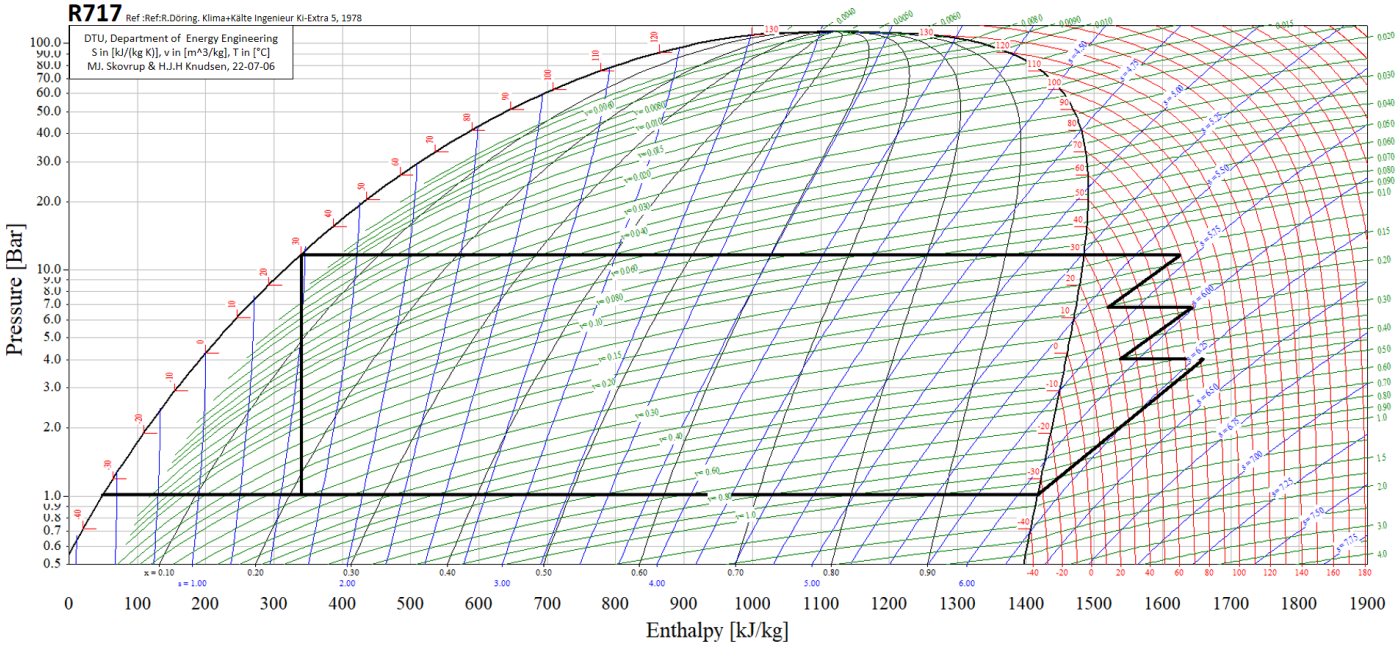

Figure 9. P–H diagrams of ammonia from 0.5 to 100 bar. The black lines illustrate the ammonia refrigeration cycle.

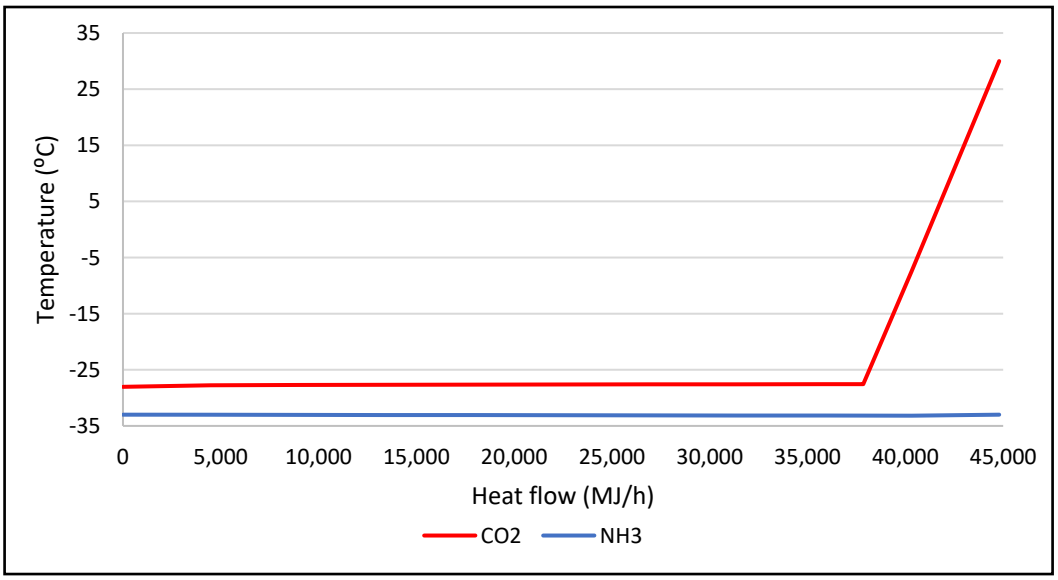

Figure 10. Heat curve for the heat exchanger. Hot composite/CO_2 stream (red) and cold composite/NH_3 (blue).

Table 6. Results for the closed-cycle liquefaction design.

Design Cases	Compressor Power (MW)	Electric Energy per Ton CO_2 (kWh/tons)	Cooling Duty (GJ/h)
7 bar (NH_3)	9.7	78.4	93.4
15 bar (NH_3)	7.5	60.5	79.7
7 bar (C_3H_8)	11.1	90.5	98.3
15 bar (C_3H_8)	8.4	68.3	83.2

3.3.2. Closed-Cycle Configuration 1

The ammonia cycle cannot be optimized by varying the high-end pressure and temperature. The 30 °C isotherm curve on the liquid side of the P–H diagram is very steep, indicating that increasing the pressure does not increase the liquid split. By decreasing the temperature of ammonia right before expansion, the liquid split can be improved. However, additional ammonia is required for the cooling process. The net power required is not improved using this method. Other process configurations are, therefore, explored.

In the first configuration, ammonia is superheated to 26 °C, before it is returned for recompression. In this design, both liquid and vapor ammonia from the valve are used to cool CO_2. See Figure 11.

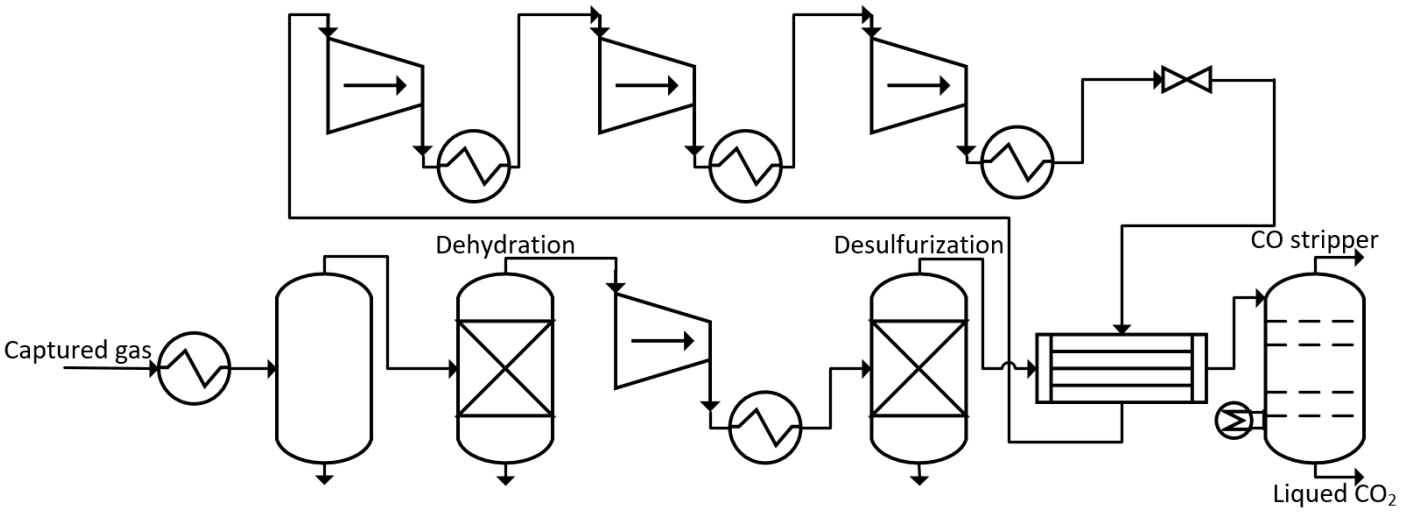

Figure 11. Process flow diagram for the closed-cycle configuration 1.

The heat curves for the closed-cycle liquefaction design configuration 1 are shown in Figure 12. As the ammonia is superheated, the two curves are better matched. Table 7 shows the results for this design.

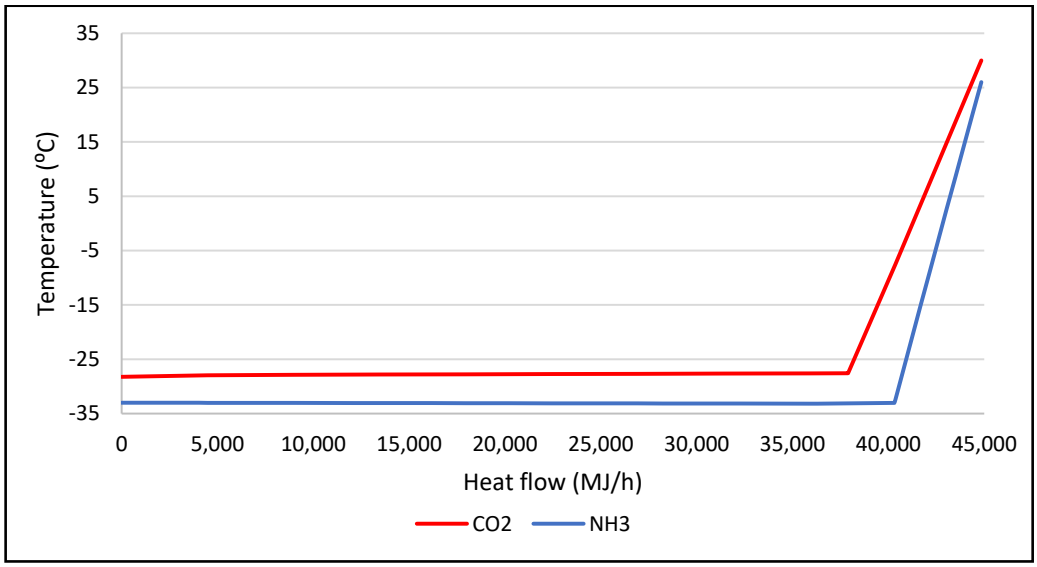

Figure 12. Heat curve for the heat exchanger. Hot composite/CO_2 stream (red) and cold composite/NH_3 (blue).

Table 7. Results for the closed-cycle configuration 1.

Design Cases	Compressor Power (MW)	Electric Energy per Ton CO_2 (kWh/tons)	Cooling Duty (GJ/h)
Closed-cycle configuration 1	7.5	61.1	80.0

It is found that superheating ammonia reduces the flow rate of ammonia because the heat curves are improved. However, because the ammonia streams are heated before they are returned to the compressors, the discharge temperatures of all compressors are increased. Since the compressor power increases with increasing discharge temperature, the overall power consumption of the process is also increased.

3.3.3. Closed-Cycle Configuration 2

In the second configuration, the liquid ammonia is superheated by CO_2, whereas the vapor ammonia is used to sub-cool itself before expansion. In that way, the liquid split of ammonia is improved. See Figure 13. However, it is also found that, in these cases, the net power consumption is not improved. See Table 8.

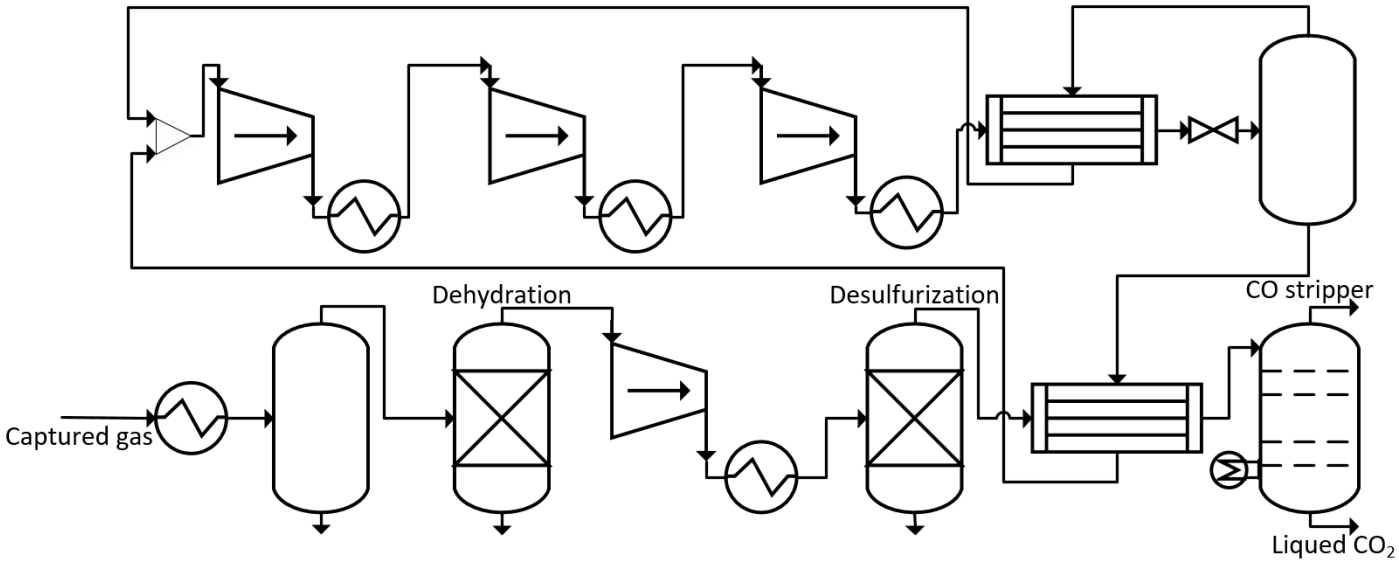

Figure 13. Process flow diagram for the closed-cycle configuration 2.

Table 8. Results for the closed-cycle configuration 2.

Design Cases	Compressor Power (MW)	Electric Energy per Ton CO_2 (kWh/tons)	Cooling Duty (GJ/h)
Closed-cycle configuration 2	7.7	62.7	80.7

3.3.4. Closed-Cycle Configuration 3

In the third configuration, the CO_2 stream is precooled using ammonia streams at intermediate temperatures, as well as the cold from the reboiler in the CO stripper. The process flow diagram of this design is shown in Figure 14.

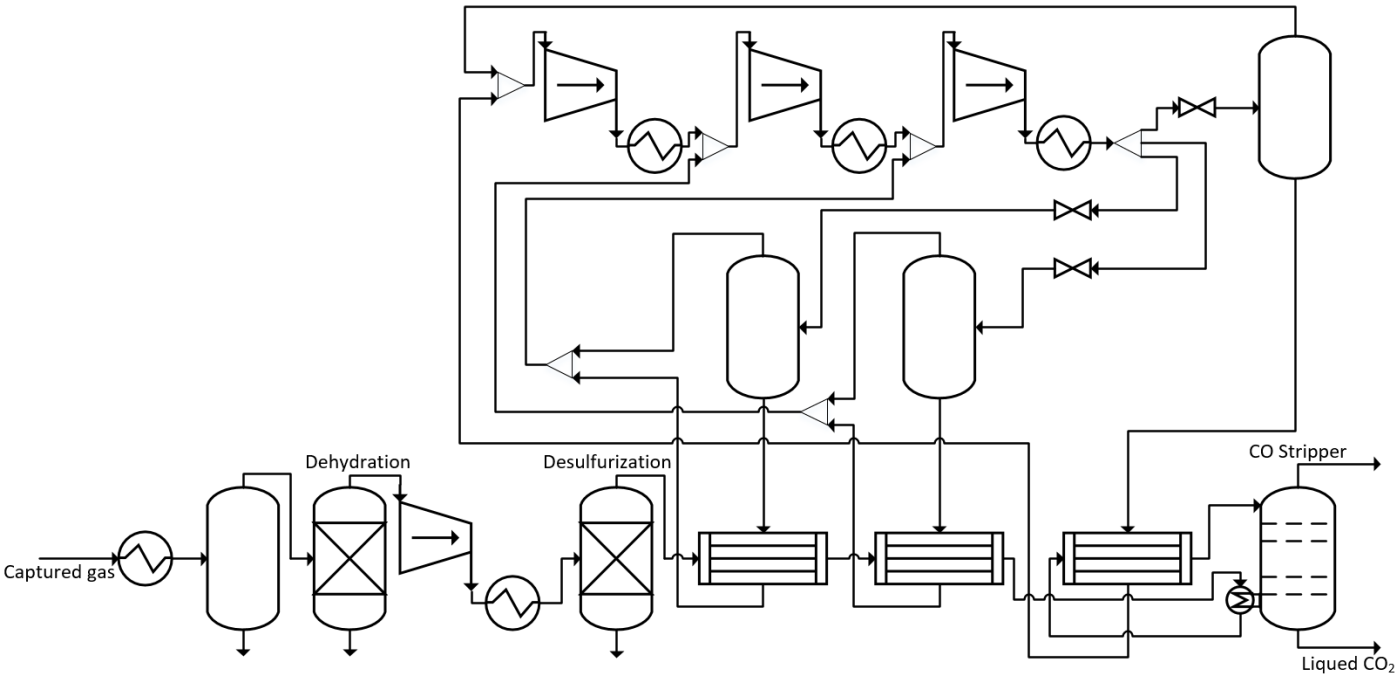

Figure 14. Process flow diagram for the closed-cycle configuration 3.

In this design, the ammonia stream is split into three streams, which expand to three different pressures:

- An ammonia stream at 6.8 bar and 13.3 °C. It is used to precool CO_2 from 30 °C to 18.5 °C. After that, it is returned to the third compressor for recompression;
- An ammonia stream at 4 bar and −1 °C. This stream is used to precool CO_2 from 18.5 °C to 3.5 °C. It is then returned to the second compressor for recompression;
- An ammonia stream at 1 bar and −33 °C. It is used to liquefy the CO_2. It is returned to the compressor for recompression.

In addition to the ammonia streams, the reboiler from the CO stripper provides extra cold, which is used to further cool CO_2 from 3.5 °C to −4.8 °C before the final liquefaction heat exchanger. The P–H diagram of ammonia in this design is shown in Figure 15.

Figure 15 shows that in the third design, three ammonia cycles are combined. The ammonia stream that operates at 1 bar undergoes three compressor stages. The stream operating at 4 bar undergoes two compressor stages, and the stream operating at 6.8 bar only undergoes one compressor stage. The cycles are combined in one system, which means that the high-end pressure for all cycles is 11.8 bar.

Figure 16 shows the heat curves of this design. Here, the heat curves are also improved compared to the base design. The two intermediate ammonia streams, indicated by the blue horizontal lines at 13.3 °C and −1.5 °C, are utilized to precool CO_2. The third heat exchanger is the reboiler of the CO stripper, and the cold from the CO stripper is utilized to precool CO_2. The blue line indicates this at −28.5 °C.

In this configuration, the total ammonia flow rate is slightly reduced from 2405 kmole/h, as in the base design, to 2350 kmole/h. The reduction in the ammonia flowrate is a result of utilizing the cold from the stripper. At the same time, the heat curve is improved without increasing the discharge temperatures of the compressors. The result of the this design is shown in Table 9.

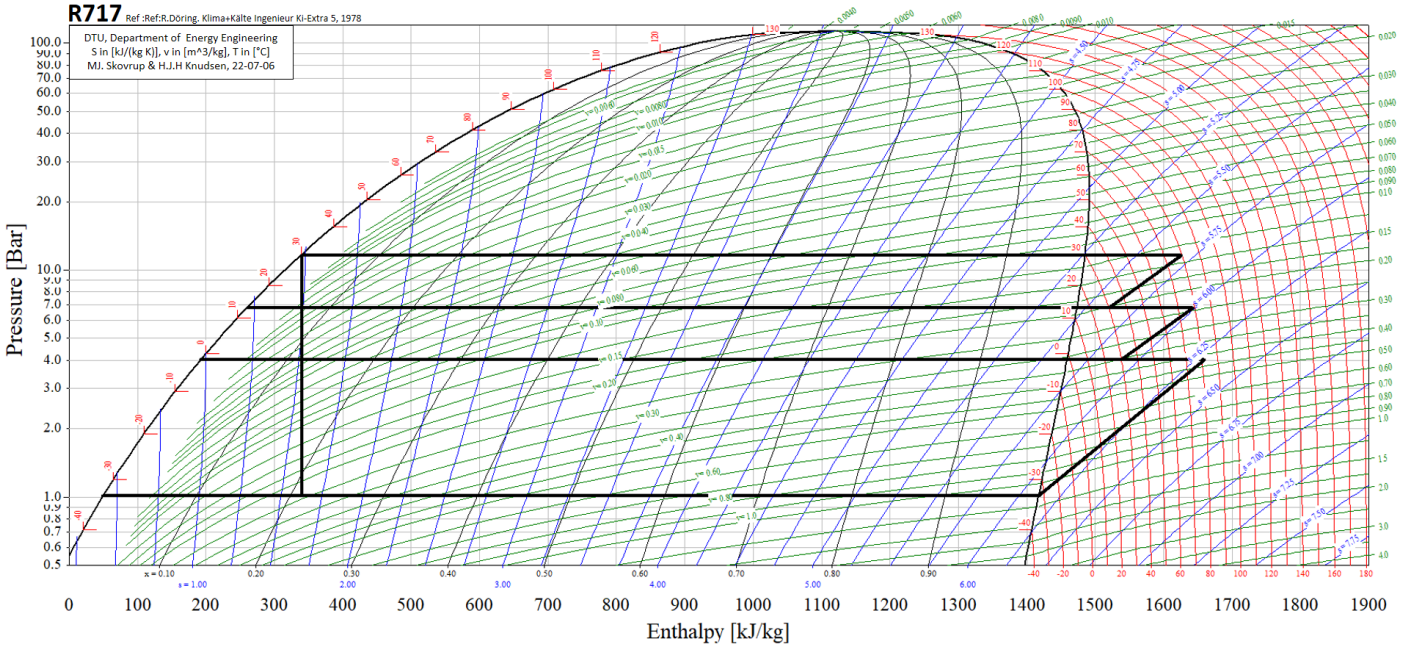

Figure 15. P–H diagram ammonia from 0.5 bar to 100 bar. The black lines illustrate the ammonia refrigeration cycle in configuration 3.

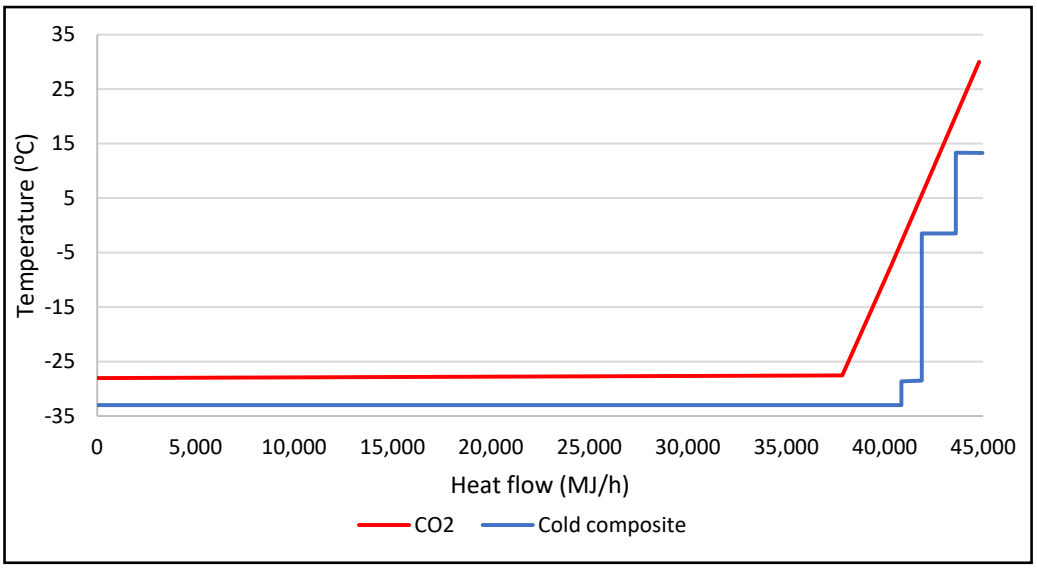

Figure 16. Heat curve of configuration 3.

Table 9. Results for the closed-cycle configuration 3.

Design Cases	Compressor Power (MW)	Electric Energy per Ton CO_2 (kWh/tons)	Cooling Duty (GJ/h)
Closed-cycle configuration 3	7.1	57.9	77.7

4. Results and Discussion

Table 10 shows the results of all designs explored in this work. Among all the designs, the process with the lowest power consumption is the ammonia process with precoolers (closed-cycle configuration 3). The total power consumption is 4.4% lower than that of the closed-cycle base design. It is worth mentioning that a different way to precool CO_2 is to use a new refrigeration cycle with a second refrigerant. Despite the fact that precooling

CO_2 is a feasible way to optimize the closed-cycle liquefaction process, constructing a new refrigeration loop with other refrigerants can be complex and costly. In the closed-cycle configuration 3, the ammonia cycle is efficiently used to produce intermediate temperature liquid ammonia streams for precooling. By doing so, the ammonia flow rates to the first two compressor stages are slightly decreased, leading to reduced power consumption.

Table 10. Summary of the results.

Design Cases	Net Power (MW)	Electric Energy per Ton CO_2 (kWh/ton)	Cooling Duty (GJ)
Open cycle with valve, 7 bar	12.8	103.6	104.1
Open cycle with valve, 15 bar	9.3	75.9	86.5
Open cycle with turbine, 7 bar	12.7	103.1	103.7
Open cycle with turbine, 15 bar	9.3	75.8	86.4
Open cycle with valve + turbine, 7 bar	10.6	85.7	96.3
Open cycle with valve + turbine, 15 bar	8.4	68,6	83.3
Closed cycle, base design, 7 bar (NH_3)	9.7	78.4	93.4
Closed cycle, base design, 15 bar (NH_3)	7.5	60.5	79.7
Closed cycle, base design, 7 bar (C_3H_8)	11.1	90.5	98.3
Closed cycle, base design, 15 bar (C_3H_8)	8.4	68.3	83.2
Closed-cycle configuration 1	7.5	61.1	80.0
Closed-cycle configuration 2	7.7	62.7	80.7
Closed-cycle configuration 3	7.1	57.9	77.7

When comparing the open and closed liquefaction cycles, it is clear that closed-cycle liquefaction is more energy efficient. However, an advantage of using the open-cycle liquefaction is to liquefy CO_2 at low pressures, which is not feasible using the closed-cycle concepts with the refrigerants investigated in this study. Even though liquefying CO_2 at low pressures can be very energy consuming, it might still be advantageous in the CCS operation, as the CO_2 transport process tends to be cheaper with lower CO_2 transport pressures. Additionally, the closed-cycle liquefaction process might have a higher CAPEX compared to the open-cycle process, as a large amount of refrigerant is required.

When comparing the refrigerants, ammonia is the best choice for 15 bar, as the designs with ammonia require 10% less compressor power than propane. However, the saturation pressure of ammonia at −33 °C is 1 atm, making it barely suitable for liquefaction, whereas for propane, the saturation pressure is 1.5 atm. Therefore, if the liquefaction pressure of CO_2 is reduced, propane can still be used as a refrigerant.

Different closed-cycle configurations are also investigated. The results show that improving the heat curves improves the net power consumption. However, superheating ammonia increases the discharge temperature of compressors, resulting in an increase in net power consumption.

5. Conclusions

In this work, the ship-based conditioning process for the 3D project is investigated. The purification technologies for water and hydrogen sulfide removal are reviewed. For the 3D project, it is recommended to use molecular sieves or adsorption technologies to remove water and activated carbon to remove H_2S. CO can be removed with a stripper. The top stream of the CO stripper is still a CO_2-rich stream, and it is suggested to recycle this stream back to the capture unit. Different designs for liquefaction are explored. By comparing the results, we find that:

- For all designs, liquefaction of CO_2 for 15 bar transport case requires much less energy than the 7 bar transport case;
- The most energy efficient open-cycle liquefaction design is to combine a turbine with a valve;

- For closed-cycle designs, both ammonia and propane are unsuitable for liquefying CO_2 at 7 bar. Additionally, using ammonia as the refrigerant is more energy efficient compared to propane;
- The most energy efficient closed-cycle liquefaction design is with precoolers, to cool CO_2 before liquefaction.

We conclude that if the transport pressure is 7 bar, the open-cycle liquefaction method shall be used. However, the power consumption for liquefying CO_2 at 15 bar with a closed-cycle design is much less than that of any open-cycle designs. Investigating the compression ratios, the minimal total compression power consumption is identified, and amounts to 57.9 kWh/ton CO_2.

Author Contributions: Conceptualization, E.R.; Formal analysis, W.G.; Investigation, W.G.; Methodology, W.G. and E.R.; Project administration, E.R., P.L.F. and N.v.S.; Supervision, E.R., P.L.F. and N.v.S.; Validation, P.L.F. and N.v.S.; Writing—original draft, W.G.; Writing—review & editing, W.G., P.L.F. and N.v.S. All authors have read and agreed to the published version of the manuscript.

Funding: This project received funding from the European Union's Horizon 2020 research and innovation program under Grant Agreement No. 838031.

Institutional Review Board Statement: Not applicable.

Informed Consent Statement: Not applicable.

Conflicts of Interest: The authors declare no conflict of interest.

References

1. Metz, B.; Davidson, O.; de Coninck, H.C.; Loos, M.; Mayer, L.A. (Eds.) *IPCC, 2005: IPCC Special Report on Carbon Dioxide Capture and Storage*; Prepared by Working Group III of the Intergovernmental Panel on Climate Change; Cambridge University Press: Cambridge, UK, 2005.
2. Mølnvik, M.J.; Aspelund, A.; Koeijer, D. Ship transport of CO_2 technical solutions and analysis of costs, energy utilization, energy efficiency and CO2 emissions. *Chem. Eng. Res. Des.* **2006**, *84*, 847–855.
3. Losnegård, S.-E.; Solvang, S.; Strømme, P.-A.; Knudsen, K.H.; Larsen, A.; Nysæterb, G.; Belgarouic, J.; Forinc, P.; Meratc, C.; Gapilloud, C. Evaluation of CO_2 storage locations and transport solutions from capture plant in Dunkirk. In Proceedings of the 15th International Conference on Greenhouse Gas Control Technologies, Abu Dhabi, United Arab Emirates, 15–18 March 2021.
4. Aspelund, A.; Jordal, K. Gas conditioning—The interface between CO2 capture and transport. *Int. J. Greenh. Gas Control* **2007**, *1*, 343–354. [CrossRef]
5. Cifre, P.G.; Brechtel, K.; Hoch, S.; Garcia, H.; Asperion, N.; Hasse, H.; Scheffnecht, G. Integration of a chemical process model in a power plant modelling tool for the simulation of an anime based CO_2 scrubber. *Fuel* **2009**, *88*, 2481–2488. [CrossRef]
6. Deng, H.; Roussanaly, S.; Skaugen, G. Techno-economic analyses of CO_2 liquefaction: Impact of product pressure and impurities. *Int. J. Refrig.* **2019**, *103*, 301–315. [CrossRef]
7. Alabdulkarem, A.; Hwang, Y.; Radermacher, R. Development of CO2 liquefaction cycles for CO_2 sequestration. *Appl. Therm. Eng.* **2012**, *33–34*, 144–156. [CrossRef]
8. Øi, L.E.; Eldrup, N.; Adhikari, U.; Bentsen, M.H.; Badalge, J.L.; Yang, S. Simulation and Cost Comparison of CO_2 Liquefaction. *Energy Procedia* **2016**, *86*, 500–510. [CrossRef]
9. Seo, Y.; Huh, C.; Lee, S.; Chang, D. Comparison of CO_2 liquefaction pressures for ship-based carbon capture and storage (CCS) chain. *Int. J. Greenh. Gas Control* **2016**, *52*, 1–12. [CrossRef]
10. Ministry of Petroleum and Energy. *Feasibility Study for Full-Scale CCS in Norway*; Ministry of Petroleum and Energy: Oslo, Norway, 2016.
11. Al Baroudi, H.; Awoyomi, A.; Patchigolla, K.; Jonnalagadda, K.; Anthony, E.J. A review of large-scale CO_2 shipping and marine. *Appl. Energy* **2021**, *287*, 116510. [CrossRef]
12. Roussanaly, S.; Deng, H.; Skaugen, G.; Gundersen, T. At what Pressure Shall CO_2 Be Transported by Ship? An in-Depth Cost Comparison of 7 and 15 Barg Shipping. *Energies* **2021**, *14*, 5635. [CrossRef]
13. Norwegian Ministry of Petroleum and Energy. *Longship—Carbon Capture and Storage*; Norwegian Ministry of Petroleum and Energy: Oslo, Norway, 2020.
14. Broutin, P.; Briot, P.; Ehlers, S.; Kather, A. Benchmarking of the DMXTM CO_2 Capture Process. *Energy Procedia* **2017**, *114*, 2561–2572. [CrossRef]
15. Raynal, L.; Alix, P.; Bouillon, P.-A.; Gomez, A.; Nailly, M.L.F.D.; Jacquin, M.; Kittel, J.; di Lella, A.; Mougin, P.; Trapy, J. The DMX™ process: An original solution for lowering the cost of post-combustion carbon capture. *Energy Procedia* **2011**, *4*, 779–786. [CrossRef]

16. Akinfiev, N.N.; Diamond, L.W. Solubility of CO_2 in water from −1.5 to 100 °C and from 0.1 to 100 MPa: Evaluation of literature data and thermodynamic modelling. *Fluid Phase Equilibria* **2003**, *208*, 265–290. [CrossRef]
17. Bauer, C.; Gros, G.; Bartels, H. *Biophysics and Physiology of Carbon Dioxide*; Springer: Berlin/Heidelberg, Germany, 1979.
18. Corroll, J.J.; Mather, A.E. The solubility of hydrogen sulphide in water from 0 to 90 °C and pressures to 1 MPa. *Geochim. Cosmochim. Acta* **1989**, *53*, 1163–1170. [CrossRef]
19. Sun, Q.; Kang, Y.T. Review on CO_2 hydrate formation/dissociation and its cold energy application. *Renew. Sustain. Energy Rev.* **2016**, *62*, 478–494. [CrossRef]
20. Ward, Z.T.; Deering, C.E.; Marriott, R.A.; Sum, A.K.; Sloan, E.D.; Koh, C.A. Phase Equilibrium Data and Model Comparisons for H_2S Hydrates. *J. Chem. Eng. Data* **2014**, *60*, 403–408. [CrossRef]
21. Kemper, J.; Sutherland, L.; Watt, J.; Santos, S. Evaluation and Analysis of the Performance of Dehydration Units for CO_2 Capture. *Energy Procedia* **2014**, *63*, 7568–7584. [CrossRef]
22. Speight, J.G. *Natural Gas*, 2nd ed.; Gulf Professional Publishing: Houston, TX, USA, 2019.
23. Abatzoglou, N.; Boivin, S. A review of biogas purification processes. *Biofuels Bioprod. Biorefin.* **2009**, *3*, 42–71. [CrossRef]
24. Villadsen, S.N.B. A Novel Electroscrubbing Process for Gas Cleaning. Ph.D. Thesis, Technical University of Denmark, Lyngby, Denmark, 2019.
25. Forster, P.; Ramaswamy, V.; Artaxo, P.; Berntsen, T.; Betts, R.; Fahey, D.; Haywood, J.; Lean, J.; Lowe, D.; Myhre, G.; et al. Changes in Atmospheric Constituents and in Radiative Forcing. In *Climate Change 2007: The Physical Science Basis*; Cambridge University Press: Cambridge, UK; New York, NY, USA, 2007.